ACS APPLIED MATERIALS & INTERFACES

Research Article

www.acsami.org

Silver Nanoparticle Gated, Mesoporous Silica Coated Gold Nanorods (AuNR@MS@AgNPs): Low Premature Release and Multifunctional Cancer Theranostic Platform

Zhehua Zhang,[†,⊥] Changhui Liu,[†,‡,⊥] Junhui Bai,[†] Cuichen Wu,[∥] Yue Xiao,[†] Yinhui Li,[†] Jing Zheng,*[,†] Ronghua Yang,*[,†,§] and Weihong Tan[†,∥]

[†]State Key Laboratory of Chemo/Biosensing and Chemometrics, College of Chemistry and Chemical Engineering, Hunan University, Changsha, 410082, China

[‡]Department of Chemistry and Environmental Engineering, Hunan City University, Yiyang, 413000, China

[§]School of Chemistry and Biological Engineering, Changsha University of Science and Technology, Changsha, 410004, China

[∥]Center for Research at the Bio/Nano Interface, Department of Chemistry and Department of Physiology and Functional Genomics, Shands Cancer Center and UF Genetics Institute, University of Florida, Gainesville, Florida 32611-7200, United States

Supporting Information

ABSTRACT: Multifunctional nanoparticles integrated with an imaging module and therapeutic drugs are promising candidates for future cancer diagnosis and therapy. Mesoporous silica coated gold nanorods (AuNR@MS) have emerged as a novel multifunctional cancer theranostic platform combining the large specific surface area of mesoporous silica, which guarantees a high drug payload, and the photothermal modality of AuNRs. However, premature release and side effects of exogenous stimulus still hinder the further application of AuNR@MS. To address these issues, herein, we proposed a glutathione (GSH)-responsive multifunctional AuNR@MS nanocarrier with in situ formed silver nanoparticles (AgNPs) as the capping agent. The inner AuNR core functions as a hyperthermia agent, while the outer mesoporous silica shell exhibits the potential to allow a high drug payload, thus posing itself as an effective drug carrier. With the incorporation of targeting aptamers, the constructed nanocarriers show drug release in accordance with an intracellular GSH level with maximum drug release into tumors and minimum systemic release in the blood. Meanwhile, the photothermal effect of the AuNRs upon application to near-infrared (NIR) light led to a rapid rise in the local temperature, resulting in an enhanced cell cytotoxicity. Such a versatile theranostic system as AuNR@MS@AgNPs is expected to have a wide biomedical application and may be particularly useful for cancer therapy.

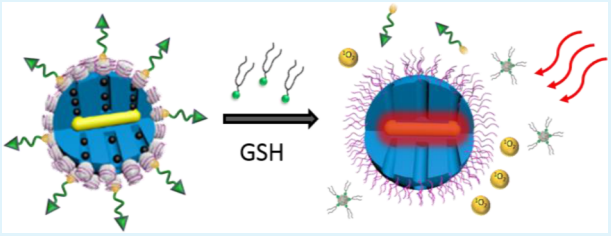

KEYWORDS: *mesoporous silica nanoparticles, gold nanorods, silver nanoparticle, GSH, photothermal therapy, photodynamic therapy*

INTRODUCTION

Nanobiotechnology, in particular methods based on nanoparticles, has made significant contributions to the improvement of drug delivery in cancer therapy over the past decades. Several types of nanoparticle-based drug delivery systems have been developed for this purpose.[1−3] Among these, the concept of multifunctional nanoparticles has attracted increasing attention.[4−8] Smart combinations of different types of functional nanomaterials, for example, by combining functional inorganic nanomaterials, including quantum dots, gold nanoparticles, magnetic particles, and carbon nanotubes, with a protective organic matrix, various multifunctional nanocarriers have been fabricated for cancer imaging, simultaneous diagnosis, and therapy.[9−12]

Recently, mesoporous silica nanoparticles (MSNs, size typically <500 nm) play an important role in cancer therapy due to their advantageous structural properties, such as high internal surface area and pore volume, tunable pore sizes, colloidal stability, and the possibility to specifically functionalize the inner pore system and/or the external particle surface.[13−17] These highly attractive features make MSNs a promising and widely applicable platform for diverse biomedical applications including diagnostic bioimaging, biosensing, and drug delivery.[18−20] Gold nanorods (AuNRs), that are one type of effective photosensitive nanomaterial and possess intense absorption bands in the near-infrared (NIR) range, have been widely applied in photothermal therapy.[21,22] Upon exposure to a NIR laser, the absorbed photon energy is converted to heat with high efficiency. Once the heat dissipates into the surroundings (i.e., the target tissue), the rise in temperature increases membrane permeability and/or promotes the destruction of biological samples. Based on the unique

Received: January 14, 2015
Accepted: February 24, 2015
Published: February 24, 2015

DOI: 10.1021/acsami.5b00368
ACS Appl. Mater. Interfaces 2015, 7, 6211−6219

Scheme 1. Schematic Illustration of Silver Nanoparticle Gated, Mesoporous Silica Coated Gold Nanorods as a New Low Premature Release and Multifunctional Cancer Theranostic Platform

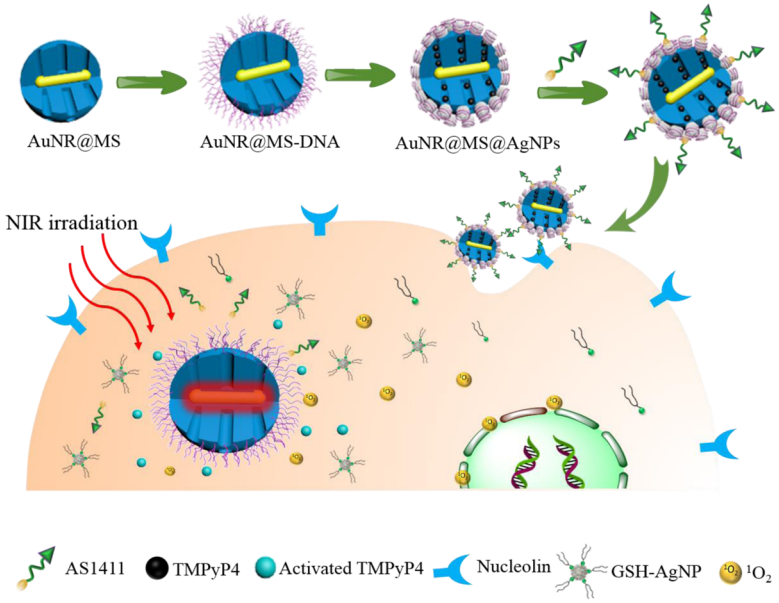

properties of these nanomaterials, mesoporous silica coated AuNR (AuNR@MS) has emerged as a novel multifunctional cancer theranostic platform combining the large specific surface area of mesoporous silica, which guarantees a high drug payload, and the photothermal modality of AuNRs.[23−26] These two therapeutic modalities are also beneficial for overcoming serious limitations encountered by each therapeutic method used alone. Taking the biocompatibility of nucleic acids into account, exploratory work on DNA gated mesoporous silica delivery systems has been carried out. Among these studies, special structured nucleic acids such as G-quadruplex and double-stranded DNA are usually chosen to serve as the gatekeepers and the capping effect is typically removed by photolysis with NIR light, photocleavage of photosensitizer hybridization with nucleic acid biomarkers, or enzyme digestion to liberate the specific DNA structure.[26−29] However, the practical application of AuNR@MS in vivo still faces some critical barriers, such as premature release due to the limited efficiency of pore blocking, and the side effects of certain high temperatures only under which the special capping DNA structure can be liberated. To address all these issues, design of an AuNR@MS drug delivery system with minimum premature release to enable the transport of an effective dosage with target recognition, especially controlled and specific intracellular release by tumor-specific endogenous stimulus for cancer treatment, is in an urgent demand.

In this paper, AuNR@MS was coated with in situ formed silver nanoparticles (AgNPs) on a DNA template to serve as the gatekeeper for drug release, as shown in Scheme 1. As the effective gatekeeper, besides low premature leakage, the decoration of AuNR@MS with AgNPs via a DNA-templated process is different from conventional covalent or noncovalent strategies, providing a less laborious but more cost-effective and robust approach to construct nanocarriers. Then, by in situ formation, the size and amount of the gatekeeper AgNPs are easily modulated by manipulating the amounts of Ag^+ ions to meet different degrees of exogenous stimulus. As a model photodynamic therapy (PDT) reagent, 5,10,15,20-tetrakis (4-*N*-methylpyridiniumyl)porphyrin ($TMPyP_4$) was loaded into AuNR@MS cavities. The emission band of $TMPyP_4$ overlapped with the longitudinal plasmon resonance absorption (LPRA) of AuNRs in our design. Due to energy transfer from the excited $TMPyP_4$ molecule to AuNRs when $TMPyP_4$ is close to the gold surface, both the fluorescence of $TMPyP_4$ and its capacity of generating singlet oxygen (SOG) could be inhibited. However, in the presence of glutathione (GSH) and thiol species, the drug release can be triggered by the constitution of ultrastable Ag−S bonds;[30−32] thus the SOG can be efficiently produced to achieve PDT. Since GSH presents a low concentration (<10 μM) in the extracellular fluid while it is relatively highly concentrated within the cytosol (1−10 mM), minimum drug leakage could be ensured in the circulatory system.[33] Meanwhile, upon irradiation with the NIR laser with a wavelength that matches the absorption peak of AuNRs, the light will be absorbed and converted into heat through the photothermal effect. To further endow AuNR@MS with high specific recognition capability, aptamer AS1411, which is specific to cancer cells with high expression of nucleolin, was decorated on the surface of this nanocarrier.[34,35] Combining with these capabilities, we have developed a multifunctional $TMPyP_4$-loaded AuNR@MS theranostic platform with two distinct functions for simultaneous therapy: targeting with aptamers and dual therapy (photodynamic/photothermal therapy). Therefore, the killing efficiency can be improved with reduced drug doses and it is expected that this versatile theranostic system will have wide biomedical applications and may be particularly useful for cancer therapy.

EXPERIMENTAL SECTION

Materials and Instruments. All oligonucleotides were synthesized by TaKaRa Biotechnology Co. Ltd. (Dalian, China). Ultrapure water obtained from a Millipore water purification system (18 MΩ) was used in all assays. *N*-Cetyltrimethylammonium bromide (CTAB), tetraethylorthosilicate (TEOS), silver nitrate ($AgNO_3$), sodium borohydride ($NaBH_4$), 1-ethyl-3-(3′-dimethylaminopropyl)-carbodiimide (EDC), *N*-hydroxysuccinimide (NHS), and 5,10,15,20-tetrakis (4-*N*-methylpyridiniumyl)porphyrin ($TMPyP_4$) were purchased from Alfa Aesar Chemical Ltd. (China). 2-(*N*-Morpholino)-

DOI: 10.1021/acsami.5b00368
ACS Appl. Mater. Interfaces 2015, 7, 6211−6219

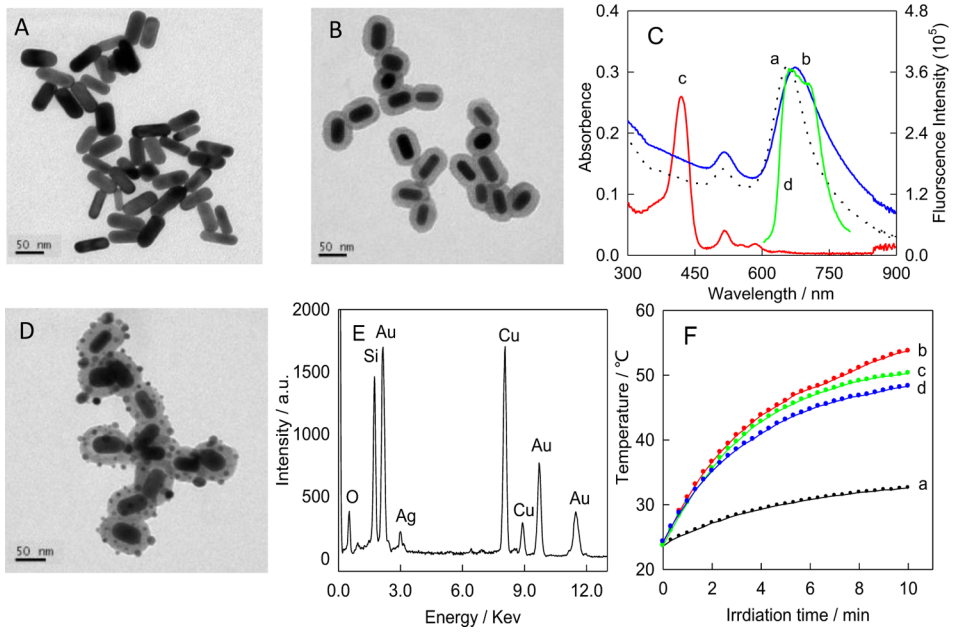

Figure 1. TEM images of (A) AuNRs and (B)AuNR@MS. (C) Absorption spectra of AuNRs (a), AuNR@MS (b), and $TMPyP_4$ (c) and emission spectrum of free $TMPyP_4$ (d). (D) TEM image of AuNR@MS@AgNPs. (E) EDX of AuNR@MS@AgNPs under the STEM pattern. (F) Temperature−time curves of PBS buffer (a), (a) + AuNR (b), (a) +AuNR@MS (c), and (a) +AuNR@MS@AgNPs (d) with 780 nm laser irradiation at 3.0 W/cm^2.

ethanesulfonic acid (MES), (3-aminopropyl)triethoxysilane (APTES), succinic anhydride, $HAuCl_4 \cdot 4H_2O$, and L-ascorbic acid were purchased from J&K Scientific. All chemicals were of analytical grade and were used as received without further purification. Human cervical carcinoma cancer cell (HeLa cell) and human hepatocyte L02 cell (L02 cell) were obtained from the American Type Culture Collection (Manassas, VA).

Preparation of AuNR@MS-P1. AuNRs, AuNR@MS, and AuNR@MS-NH_2 were synthesized according to the published procedure with some minor modifications.[23,36] The as-synthesized AuNR@MS-NH_2 was further reacted in NH_4NO_3−ethanol solution to remove the surfactant template CTAB.[37] AuNR@MS-COOH were obtained by reacting AuNR@MS-NH_2 with succinic anhydride.[38] The conjugation between P1 and AuNR@MS-COOH was based on the EDC/NHS method.[26] Experimental details are shown in the Supporting Information.

Drug Loading. AuNR@MS-P1 and $TMPyP_4$ solutions were mixed together and stirred at room temperature for 1 day to reach the equilibrium state. The $TMPyP_4$-loaded AuNR@MS-P1 (AuNR@$TMPyP_4$@MS-P1) was collected by centrifugation at 12 000 rpm for 3 min and then washed three times with water to remove the physically adsorbed $TMPyP_4$. The amount of loaded drug for AuNR@MS was determined by fluorescence spectroscopy at 660 nm (one of the characteristic emission wavelengths of $TMPyP_4$). The fluorescence maximums were converted to molar concentrations by interpolation from a standard linear calibration curve. Standard curves were prepared with known concentrations of $TMPyP_4$ using identical buffer pH and salt concentrations. The drug loading content and entrapment efficiency were calculated by the following equation: loading content = (weight of $TMPyP_4$ in AuNR@MS)/(weight of AuNR@MS).

Preparation of AuNR@MS@AgNPs. The procedure was carried out according to the previous work in our laboratory.[39] Briefly, 1 mg of AuNR@$TMPyP_4$@MS-P1 was dispersed in 6 mL of Milli-Q water and cooled at 4 °C for 1 h followed by the addition of $AgNO_3$ (115.5 μL, 4 mM) under gentle shaking and then cooled at 4 °C for another hour followed by the addition of ice-cold $NaBH_4$ (57.7 μL, 20 mM). The mixture was then placed at 4 °C overnight to fulfill the growth of AgNPs. The concentration of $NaBH_4$ exceeded that of $AgNO_3$ by 2.5 times.

In Vitro Test of Drug Release. A sample of 0.25 mg of AuNR@$TMPyP_4$@MS@AgNPs was placed in a closed dialysis bag in a 10 mL plastic tube containing 2 mL of phosphate buffer (25 mM, pH 7.4) with different GSH concentrations. The releasing experiments were carried out under gentle stirring in a dark environment, and the released $TMPyP_4$ was calculated through detecting the fluorescence of the supernatant solution at 1 h intervals.

Evaluation of SOG. To evaluate the SOG generation of samples, Singlet Oxygen Sensor Green (SOSG) was introduced at a concentration of 6.0 μM using 50% D_2O in 20 mM Tris·HCl buffer as solvent. The SOSG fluorescence was read with the excitation at 504 nm and the maximum emission at 534 nm after the irradiation. SOG induced by $TMPyP_4$ was measured after the sample was irradiated by white light for 20 min.

Preparation of AuNR@MS@AgNPs-AS1411. Initially, thiolated AS1411 aptamer (1.0 mM) was reduced by tris(2-carboxyethyl)-phosphine (1.0 mM, freshly prepared) in acetate buffer (50 mM, pH 5.2) for 1 h at room temperature. Then, freshly activated AS1411 aptamer (1.0 μL, 10 μM) was added to AuNR@MS@AgNPs suspension (2.0 mL, 1.0 mg/mL) with gentle hand shaking. The mixture was magnetically stirred at room temperature overnight. After brief vortexing, the solution was stored at room temperature for 24 h. The supernatant was removed by centrifugation at 10 000 rpm for 5 min, and AuNR@MS@AgNPs@AS1411 were obtained by drying under high vacuum.

Internalization of AuNR@$TMPyP_4$@MS@AgNPs-AS1411. First, cells were incubated with AuNR@$TMPyP_4$@MS@AgNPs-AS1411 or AuNR@$TMPyP_4$@MS@AgNPs-random DNA (both labeled with fluorescein, FAM) at 4 or 37 °C for 2 h. They were then washed with 1 mL of washing buffer to remove the unbound nanoparticles and, then, incubated with trypsin (500 μL, 0.05%)/EDTA (0.53 mM) in HBSS (Hank's balanced salt solution) at 37 °C for 10 min. After the incubation, the cells were washed twice with 1 mL of washing buffer and suspended in binding buffer (100 μL with 0.1% NaN_3) for the flow cytometric analysis and confocal imaging.

Confocal Fluorescence Imaging. HeLa or L02 cells (10^5 cells/well) were seeded in 35 mm plastic-bottomed dishes and grown in cell culture medium supplemented with 10% fetal calf serum (FBS) and incubated under 5% CO_2 atmosphere at 37 °C for 24 h. The cells were washed three times with washing buffer and then pretreated with

DOI: 10.1021/acsami.5b00368
ACS Appl. Mater. Interfaces 2015, 7, 6211−6219

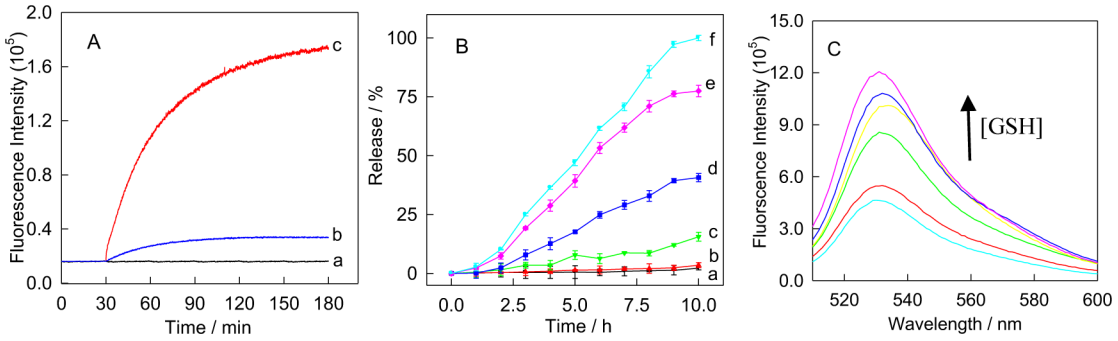

Figure 2. (A) Real-time records of the fluorescence emission at 660 nm (λ_{ex} = 421 nm), reflecting changes of the AuNR@TMPyP$_4$@MS@AgNPs in PBS (a), in PBS containing 50% human serum (b), and (b) + 5.0 mM GSH (c). (B) Cumulative release of TMPyP$_4$ from AuNR@TMPyP$_4$@MS@AgNPs triggered by different amounts of GSH. (C) Fluorescence spectrum of SOSG of AuNR@TMPyP$_4$@MS@AgNPs upon different amounts of GSH addition (λ_{ex} = 504 nm; the arrow indicates concentrations of GSH from bottom to top: 0 μM, 10 μM, 1 mM, 5 mM, 8 mM, and 10 mM).

glutathione monoester (GSH-OEt, 5.0 mM) or *N*-methylmaleimide (NMM, 5.0 mM) to regulate the concentration of intracellular GSH in 5% CO_2 at 37 °C for 2.0 h, respectively. After the cells were washed twice with washing buffer and replaced with fresh medium, AuNR@TMPyP$_4$@MS@AgNPs-AS1411 was added at the concentration of 100 μg/mL, and the mixture was incubated for different times in 5% CO_2 at 37 °C. The cells were then washed twice with washing buffer (4.5 g/L glucose and 5 mM $MgCl_2$ in Dulbecco's phosphate buffered saline (PBS) with calcium chloride and magnesium chloride) and visualized under a laser scanning confocal microscope.

Cell Culture and Viability Assay. The cytotoxicity was investigated by MTT assay for HeLa and L02 cell lines in a 96-well plate. HeLa or L02 cells (5×10^4 cells/well) were treated with serial concentrations of free TMPyP$_4$, AuNR@MS@AgNPs, AuNR@MS@AgNPs-AS1411, and AuNR@TMPyP$_4$@MS@AgNP-AS1411.The cells were incubated for 24 h to fulfill the release of TMPyP$_4$ in nanoparticles. For photodynamic therapy (PDT), the cells were put on ice for 3 h with the irradiation of white light (40 W); for photothermal therapy (PTT), the cells were irradiated with a 3.0 W/cm^2 NIR laser (780 nm). After irradiation, cells were then incubated at 37 °C under 5% CO_2 for 24 h, during which cells grew in log phase. Finally, 60 μL of MTT solution (1 mg/mL) in RPMI-1640 medium solution was added to each well and incubated at 37 °C for 2 h. The precipitated formazan violet crystals were dissolved in 150 μL of DMSO. The absorbance of formazan was measured at 570 nm by an ELISA reader. Each experiment was repeated at least three times.

RESULTS AND DISCUSSION

Characterization of AuNR@MS@AgNPs. AuNRs were prepared using the seed-mediated method proposed by Kagan et al. with slight modifications.[40] Transmission electron microscopy (TEM) images showed the average length and width of the AuNRs were about 46 and 19 nm, respectively (Figure 1A). The modified sol–gel method was then employed for the preparation of AuNR@MS.[36] The surface of AuNR@MS was functionalized with 3-aminopropyltriethoxysilane to attain AuNR@MS-NH_2, which was then reacted with succinic anhydride to produce AuNR@MS-COOH.[26,38] Zeta (ζ) potential measurements (Supporting Information, Figure S1a–d) and Fourier transform infrared (FT-IR) analysis (Supporting Information, Figure S2) provided evidence of the modification of amino and carboxyl groups. As shown in Figure 1B, the dark contrast AuNRs were clearly encapsulated by the silica shell showing light contrast. More importantly, from TEM images of the synthesized AuNR@MS, the amorphous silica shell was estimated to have a homogeneous thickness of about 15 nm and composed of disordered mesopores of about 3 nm in diameter, offering an opportunity for AuNR@MS to be used as a general drug carrier. The AuNR@MS-COOH were then functionalized with a 25-mer Ag^+-specific single-stranded DNA scaffold (P1, 5′-NH_2-CCCCTAACCCTAACCCTAACCCTAA-3′), to form AuNR@MS-P1. The decreased ζ potential from −20.0 to −27.2 mV (Supporting Information, Figure S1e) suggested that P1 had been successfully attached to the surface of AuNR@MS (AuNR@MS-P1) in a covalent manner. Meanwhile, from the UV–vis absorption spectrum we can see that the as-prepared AuNRs have a longitudinal surface plasmon resonance (SPR) peak at 658 nm (curve a, Figure 1C) which indicates the potential of photothermal conversion. After silica-shell coating, it exhibits a small red shift (about 26 nm) due to the local increase of refractive index and the scattering from the silica shells (curve b, Figure 1C), which overlaps the emission band of the subsequent loaded TMPyP$_4$ (the absorption peaks of TMPyP$_4$ are at 421, 516, and 584 nm with emission at 660 nm; see curves c and d, respectively, in Figure 1C). Since the LPRA of AuNRs overlapped with the emission band of TMPyP$_4$, the fluorescence of TMPyP$_4$ could be inhibited due to energy transfer from the excited TMPyP$_4$ to AuNRs when TMPyP$_4$ was close to the gold surface, as well as reducing the generation of SOG for PDT. The SOG was quantified with the fluorescence intensity of Singlet Oxygen Sensor Green (SOSG), which can be specifically oxidized by SOG to produce enhanced fluorescence upon oxidation.[41] The quenching experiment was performed by sequential addition of increasing fractions of AuNRs to TMPyP$_4$, and the fluorescence emission of the resultant solution was recorded. As shown in the Supporting Information, Figure S3, the fluorescence of TMPyP$_4$ was gradually quenched with increasing equivalences of AuNRs and the SOSG signal of TMPyP$_4$ in 50% D_2O buffer was quenched upon addition of AuNRs. To load TMPyP$_4$ into the mesporous shell, AuNR@MS-P1 was dispersed into TMPyP$_4$ solution under gentle shaking to reach the equilibrium state. Then, the mixtures were centrifuged to remove the excess unloaded TMPyP$_4$. With the collection of supernatants, the fluorescence intensity of the supernatants was tested. According to a standard curve of TMPyP$_4$ (data not shown), we calculated that the loading of TMPyP$_4$ in AuNR@MS-P1 is 19.3 nmol/mg.

After TMPyP$_4$ was loaded into AuNR@MS-P1 cavities, AgNPs were formed by reducing the AuNR@MS-P1/Ag^+ mixture ($n$$Ag^+$:$n$P1 = 60:1) with $NaBH_4$ aqueous solution. As shown in Figure 1D, dark spots on the outside edges of the mesopores, representing the aggregation of AgNPs on the exterior surface of AuNR@MS, could be clearly visualized. This

DOI: 10.1021/acsami.5b00368
ACS Appl. Mater. Interfaces 2015, 7, 6211–6219

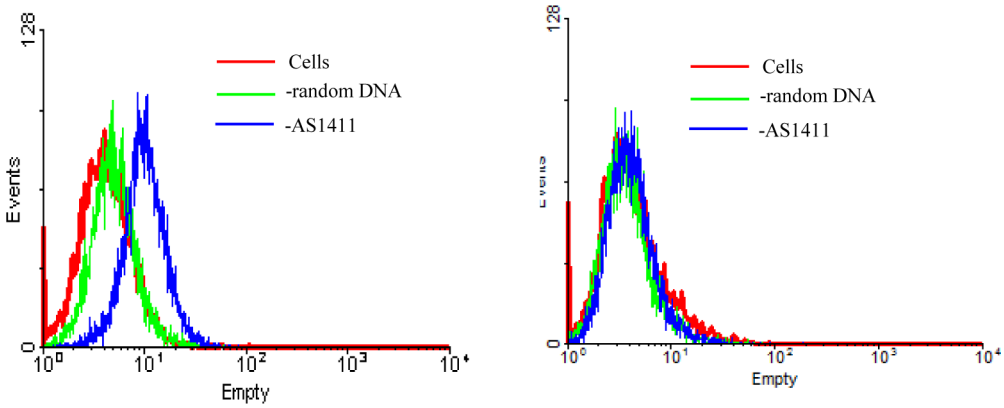

Figure 3. Flow cytometric assay to monitor the specific binding of FITC-labeled AuNR@MS@AgNPs-random DNA and AuNR@MS@AgNPs-AS1411 to the target HeLa cells (A) and the control L02 cells (B) at 4 °C for 0.5 h. Cells, 50k/sample.

event was accompanied by a remarkable increase of ζ potential (Supporting Information, Figure S1f). The presence of AgNPs was also further confirmed by energy-dispersive X-ray (EDX) spectroscopy analysis, and the coexistence of Au, Si, and Ag elements could be observed (Figure 1E). These collective results demonstrated the successful formation of DNA-templated AuNR@MS@AgNPs. In addition, the efficiency of photoinduced temperature increases in the solution from the AuNR@MS@AgNPs colloids was further investigated as a function of irradiation time using a continuous-wave (CW) NIR laser. A thermocouple was used to measure the bulk solution temperature, and the results show that the solution temperature was gradually raised as the irradiation time was prolonged while the temperature of the solution without AuNR@MS@AgNPs did not increase appreciably (Figure 1F). These results indicate that it is an absorbent of NIR light for photothermolysis in cancer therapy.

In Vitro Drug Release of AuNR@TMPyP$_4$@MS@AgNPs. To demonstrate GSH-triggered uncapping of AgNPs from the AuNR@MS@AgNPs surface and the resultant controlled drug release, the recovery fluorescence of $TMPyP_4$ from AuNR@$TMPyP_4$@MS@AgNPs was determined. Since GSH presents a low concentration (<10 μM) in the extracellular fluid while it is relatively highly concentrated within the cytosol (1−10 mM), our constructed AuNR@$TMPyP_4$@MS@AgNPs was highly anti-interferential against biological complexes and minimum drug leakage could be expected in the circulatory system. As shown in Figure 2A, the fluorescence of $TMPyP_4$ in the AuNR@MS@AgNPs conjugate showed very weak change in 50% human serum (Figure 2A, curve b), indicating that the AgNPs can keep efficient pore blocking in the biological complex. However, an intense fluorescence increase could be observed upon the addition of 5 mM GSH (Figure 2A, curve c), which demonstrated an ideal $TMPyP_4$ release triggered by GSH. To further investigate the controlled cargo release, in vitro release experiments of the $TMPyP_4$-loaded AuNR@MS@AgNPs systems with different concentrations of GSH were performed, as shown in Figure 2B. In the absence of GSH, only small amounts of $TMPyP_4$ were released into the solution under stirring for 10 h, signifying the efficient confinement of the drug in the pores of the AuNR@MS by AgNPs capping. More importantly, 10 μM GSH induced a relatively slow release, and less than 4% $TMPyP_4$ was released over a period of 10 h, while 5.0 mM GSH, which represents the intracellular GSH concentration, can lead to a burst release of the drug,[33] with a maximal cumulative release of ~41% reached within 10 h. When the GSH concentration increased to 10 mM, almost 100% $TMPyP_4$ release could be achieved. In addition, the SOSG signal was enhanced by the addition of different concentrations of GSH which allowed $TMPyP_4$ to move away from the AuNRs surface, as shown in Figure 2C. These results indicated that the $TMPyP_4$ released from the nanocarriers was dependent on the GSH level and higher concentrations of GSH could cause a stronger SOSG enhancement, proving that SOG can be efficiently generated to achieve PDT. Meanwhile, a tripeptide which has the same molecular backbone as GSH but without sulfydryl was investigated as a control experiment. As shown in the Supporting Information, Figure S4, we can observe negligible fluorescence changes upon the addition of tripeptide, which further confirmed that the mercaptan group was the key factor to trigger the detachment of AgNPs from AuNR@MS.

Since the AgNPs capped on the surface of AuNR@MS were formed by in situ reduction of the bound Ag^+, the particle size, shape, and amounts of the AgNPs can be easily modulated by varying the concentration of $AgNO_3$ to meet the different degrees of GSH stimuli and thus satisfy the requirement for target-induced drug release at different locations. In our design, two additional types of AgNP-capped AuNR@MS with concentration ratios of Ag^+ to P1 of 40:1 and 80:1 were prepared, respectively, and GSH-triggered $TMPyP_4$ release of all three $TMPyP_4$−AuNR@MS systems was determined. Figure S5 in the Supporting Information shows an evident fluorescence signal was observed in the present of 50% human serum when the concentration ratio between Ag^+ and P1 was 40:1, indicating an undesirable premature drug release of our constructed nanocarrier. When the ratio of Ag^+ to P1 increased to 60:1, weak fluorescence observed in PBS demonstrated that most $TMPyP_4$ was encapsulated within the AuNR@MS under neutral aqueous condition without any premature release. Meanwhile, the fluorescence intensity of $TMPyP_4$ was found to be slightly increased upon addition of 50% human serum, indicating that only a little $TMPyP_4$ was released into the solution in a complex biological sample in the absence of GSH, and thus demonstrating efficient confinement of drug in the pores of the AuNR@MS with AgNPs capping. Upon 5.0 mM GSH addition, the fluorescence signal of the system became stronger, indicating the substantial release of $TMPyP_4$ by uncapping of AgNPs. Finally, with further increasing the ratio of Ag^+ to P1 to 80:1, we could observe

DOI: 10.1021/acsami.5b00368
ACS Appl. Mater. Interfaces 2015, 7, 6211−6219

the system did not give a better fluorescence response to GSH than that of Ag^+ to P1 of 60:1 under identical conditions. Therefore, considering the premature leakage in the complex biological sample and biomolecule-triggered release upon GSH addition, the optimal concentration ratio of Ag^+ to P1 was chosen as 60:1 in the subsequent experiment.

Specific Binding and Internalization of AuNR@TMPyP$_4$@MS@AgNPs-AS1411. To provide the binding specificity of these constructed AuNR@MS@AgNPs, fluorescein isothiocyanate (FITC) labeled AS1411 aptamer and random DNA were anchored onto the surfaces of AgNPs via the thiol end to yield AuNR@MS@AgNPs-AS1411 and AuNR@MS@AgNPs-random DNA, respectively. A noticeable change in the fluorescence signal between AuNR@MS@AgNPs, AuNR@MS@AgNPs-random DNA, and AuNR@MS@AgNPs-AS1411 labeling HeLa cells indicated the binding capability of AuNR@MS@AgNPs-AS1411 (Figure 3A). No significant change of fluorescence intensity was observed for L02 cells, a control cell line which did not bind with the AS1411 aptamer (Figure 3B), further confirming the specific recognition of the AuNR@MS@AgNPs-AS1411 for targeted HeLa cells.

We proceeded to characterize the internalization of the constructed AuNR@MS@AgNPs-AS1411. The cells were then treated with trypsin at 37 °C to remove the external binding fluorescence signal that could interfere with the detection of the intracellular AuNR@MS@AgNPs-AS1411. In previous studies with aptamer AS1411, our research group found that trypsin treatment is an simple method to remove cell-surface-bound aptamers in the assays of flow cytometry and internalization.[42] After trypsin treatment, the fluorescence signal from flow cytometry for HeLa cells was very weak at 4 °C, but still showed a high fluorescence signal at 37 °C, as shown in the Supporting Information, Figure S6, which can be attributed to the binding of aptamer to the cell membrane protein at 4 °C and the internalization at 37 °C, clearly demonstrating the internalization of AuNR@MS@AgNPs-AS1411 into HeLa cells.

Intracellular Drug Release of AuNR@TMPyP$_4$@MS@AgNPs-AS1411. To demonstrate that the intracellular release of TMPyP$_4$ from AuNR@TMPyP$_4$@MS@AgNPs-AS1411 was effectively induced by GSH, confocal laser scanning microscopy was performed to investigate the up-capping capabilities of different GSH levels. As controls, GSH-OEt, a GSH synthesis enhancer,[43] and NMM, a GSH scavenger,[44] were used to upregulate and downregulate the GSH level in HeLa cells, respectively. In contrast to the regular HeLa cells without treatment, the fluorescence signal of AuNR@TMPyP$_4$@MS@AgNPs-AS1411 to HeLa cells could be significantly enhanced after treatment with GSH-OEt and drastically decreased with NMM (Figure 4A), suggesting that the release of TMPyP$_4$ was factually resulted from the high concentration of cytosolic GSH.

We also used flow cytometry to collect fluorescence data for HeLa cells treated with AuNR@TMPyP$_4$@MS@AgNPs-AS1411 under different conditions. The result is demonstrated in Figure 4B. Compared with confocal laser scanning microscopy, which allows imaging only a small number of cells, flow cytometry can analyze thousands of cells per second, generating a quantifiable statistical average for a large population of cells, while eliminating cell-to-cell variation and experimental artifacts. The flow cytometry results were in excellent agreement with the confocal imaging; about 2-fold

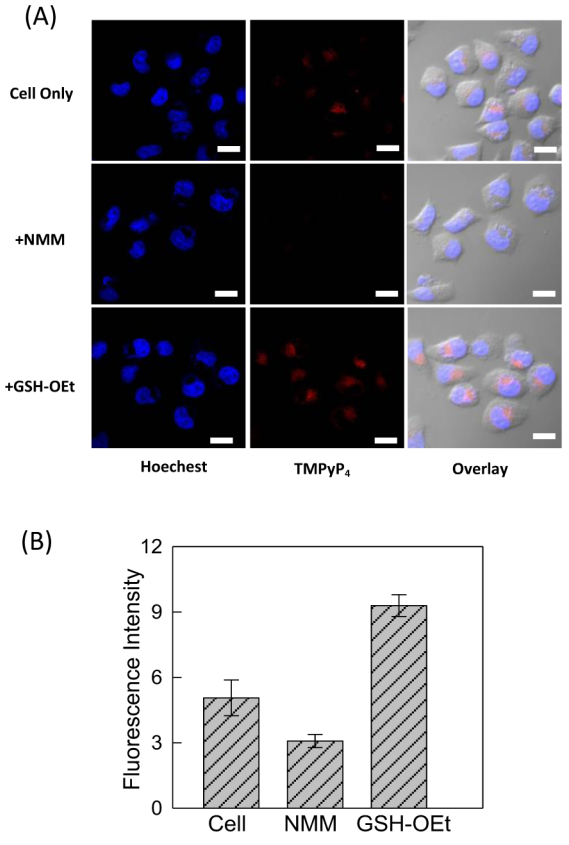

Figure 4. Intracellular TMPyP$_4$ release of AuNR@TMPyP$_4$@MS@AgNPs-AS1411 in HeLa cells under different conditions. (A) Confocal microscopy fluorescence imaging of HeLa cell populations without GSH-OEt or NMM addition (a), treated with 3 μg/mL NMM (b), and treated with 100 μM GSH-OEt (c), followed by incubation with AuNR@TMPyP$_4$@MS@AgNPs. The red pseudocolor represents the intracellular TMPyP$_4$ released triggered by GSH, and cell nuclei were stained with Hoechest 33342. Scale bar: 20 μm. (B) Flow cytometry results from HeLa cells without GSH-OEt or NMM addition (a), treated with 3 μg/mL NMM (b), and treated with 100 μM GSH-OEt (c), followed by incubation with AuNR@TMPyP$_4$@MS@AgNPs.

enhancement was observed for HeLa cells co-incubated with GSH-OEt. Taken together, it was confirmed that the release of the encapsulated drugs could be attributed to the intracellular GSH.

Cytotoxicity of AuNR@TMPyP$_4$@MS@AgNPs-AS1411. To assess the performance of cancer therapy of our targeted drug delivery system, we investigated the in vitro cytotoxicity of AuNR@MS@AgNPs-AS1411 only, TMPyP$_4$ only, and AuNR@TMPyP$_4$@MS@AgNPs-AS1411 for HeLa cell and L02 cells, respectively. To accomplish this, cells were incubated with AuNR@MS@AgNPs-AS1411, free TMPyP$_4$, or AuNR@TMPyP$_4$@MS@AgNPs-AS1411 and then exposed to a white light. Both normal and cancer cells showed high cell viability (above 90%) after incubation with a series of concentrations of AuNR@MS@AgNPs/AS1411 only upon white light irradiation, indicating that our drug delivery system has excellent biocompatibility (Supporting Information, Figure S7). TMPyP$_4$ only and AuNR@TMPyP$_4$@MS@AgNPs-AS1411 exhibited dose-dependent cytotoxicity behavior to HeLa cells, as well as L02 cells. Figure 5A shows that the inhibition concentration (half-maximal inhibitory concentration of a substance, IC_{50}) of AuNR@TMPyP$_4$@MS@AgNPs-AS1411 to HeLa cells was 1.3 μM, which is much lower than that for TMPyP$_4$ (IC_{50} = 5.0

DOI: 10.1021/acsami.5b00368
ACS Appl. Mater. Interfaces 2015, 7, 6211−6219

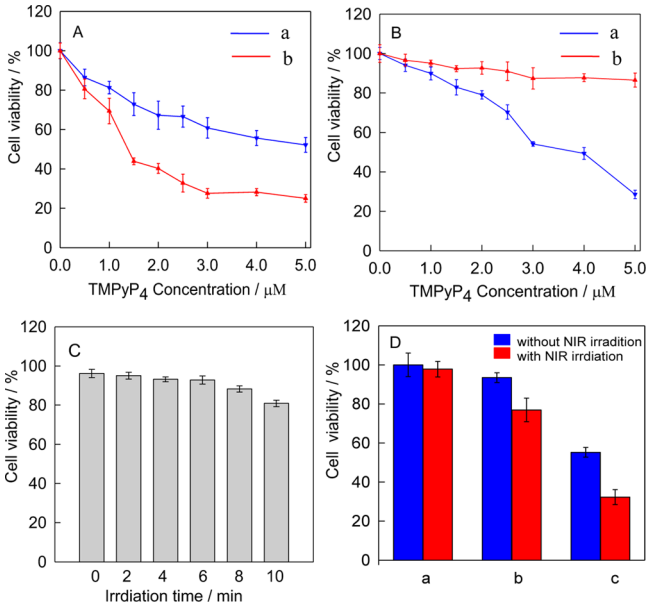

Figure 5. Cytotoxicity of AuNR@TMPyP$_4$@MS@AgNPs-AS1411. Cytotoxicity assay of HeLa cells (target cells, A) and L02 cells (control cells, B) treated with free TMPyP$_4$ (a) and AuNR@TMPyP$_4$@MS@AgNPs-AS1411 (b). (C) Cytotoxicity assay of HeLa cells treated with AuNR@MS@AgNPs-AS1411 with laser irradiation for different duration times. NIR irradiation was conducted with a 780 nm continuous-wave laser at 3.0 W/cm^2. (D) Combination of photothermal and photodynamic therapies of HeLa cells. Cells only (a); (a) + AuNR@MS@AgNPs-AS1411 (b); (a) + AuNR@TMPyP$_4$@MS@AgNPs-AS1411 (c). Concentrations of AuNR@MS@AgNPs-AS1411 and AuNR@TMPyP$_4$@MS@AgNPs-AS1411 were 100 μg/mL. The 780 nm laser irradiation was at the dose of 3.0 W/cm^2 for 10 min.

μM), demonstrating that encapsulating TMPyP$_4$ into AuNR@MS@AgNPs-AS1411 enhanced the killing efficacy of TMPyP$_4$ to HeLa cells. For L02 cells, the cell viability of 49.3 ± 2.9% with TMPyP$_4$-only treatment (4.0 μM) increased to 87.7 ± 2.0% with AuNR@TMPyP$_4$@MS@AgNPs-AS1411 treatment, as shown in Figure 5B. This can be attributed to the lack of nucleolin expression on the surface of L02 cells, indicating that nonspecific uptake of TMPyP$_4$ was minimized by the formation of a stable AuNR@TMPyP$_4$@MS@AgNPs-AS1411 conjugate. The cytotoxicity results demonstrated that the drug delivery system has excellent selectivity compared to conventional PDT using TMPyP$_4$ only, an important benefit to reduce the side effects of photodynamic therapy.

To further prove that AuNR@MS@AgNPs-AS1411 can also be used for PTT, cell death after treatment with TMPyP$_4$ only, AuNR@MS@AgNPs-AS1411 only, and AuNR@TMPyP$_4$@MS@AgNPs-AS1411, with or without laser irradiation, was determined by using the MTT assay method. A control experiment by directly illuminating HeLa cells alone without TMPyP$_4$ or AuNR@MS@AgNPs-AS1411 treatment for different NIR light irradiation duration times was first conducted, and negligible toxicity was observed, demonstrating the laser biocompatibility (Supporting Information, Figure S8). It is also worth noting after TMPyP$_4$-only treatment and without white light irradiation, the viability of HeLa cell or L02 cells remains largely unchanged upon laser irradiation,which indicates the photosensitizer cannot be excited by NIR light (Supporting Information, Figure S9). Then, HeLa and L02 cells incubated with AuNR@MS@AgNPs-AS1411 were exposed to NIR light illumination at 3.0 W/cm^2 for 10 min. Irradiation of HeLa cells with AuNR@MS@AgNPs-AS1411 increased the temperature to 44.6 °C, while L02 cells incubated with AuNR@MS@AgNPs-AS1411 only reached 36.1 °C (Supporting Information, Figure S10). The MTT results show an increased number of HeLa cells were killed by AuNR@MS@AgNPs-AS1411 after laser illumination for different times by the specific binding of AuNR@MS@AgNPs-AS1411 to targeted cells, coupled with a photothermal effect (Figure 5C).

Finally, to demonstrate the multimodal effect of our constructed drug delivery system, the viability of HeLa cells fells to under 32% when used for both PDT and PTT with incubation of AuNR@TMPyP$_4$@MS@AgNPs-AS1411 at a concentration of 100 μg/mL, indicating that AuNR@TMPyP$_4$@MS@AgNPs-AS1411 can destroy cancer cells more efficiently (Figure 5D). In contrast, PDT/PTT cytotoxicity to nontarget L02 (Supporting Information, Figure S11) cells was negligible, with cell viability of about 85%. Therefore, the synergistic effect between TMPyP$_4$ and NIR irradiation can be well demonstrated so that nonspecific toxicity and side effects can be minimized.

CONCLUSIONS

In summary, we have developed a low premature release and multifunctional AuNR@MS nanocarrier with in situ formed AgNPs as the capping agent for photothermal and photodynamic cancer therapy. A photodynamic therapy reagent, TMPyP$_4$, was then successfully incorporated into the obtained AuNR@MS@AgNPs. Aptamer AS1411, which is specific to cancer cells with high expression of nucleolin, was decorated on this nanocarrier to further endow AuNR@MS with high specific recognition capability. After cellular internalization, efficient TMPyP$_4$ release within targeted cells can increase intracellular drug concentration and thus encourage cell apoptosis. In addition, when exposed to NIR irradiation, the photothermal effect of AuNRs can lead a rapid rise in the local temperature. Therefore, the result shows that a synergistic effect in killing cancer cells was found by the combined photothermal therapy and photodynamic cancer therapy. This design might find potential applications in new drug development, existing drug improvement, and drug delivery for cancer therapy.

ASSOCIATED CONTENT

Supporting Information

ζ potential and FT-IR spectra of the synthesized nanoparticles; inhibition of AuNRs on TMPyP$_4$ for the generation of SOG; glutathione selectivity; optimization of Ag$^+$:P1 ratios; flow cytometry data; cytotoxicity of free TMPyP$_4$ by NIR irradiation; cytotoxicity of AuNR@MS@AgNPs-AS1411and AuNR@TMPyP$_4$@MS@AgNPs-AS1411 on L02 cells, etc. This material is available free of charge via the Internet at http://pubs.acs.org.

AUTHOR INFORMATION

Corresponding Authors

*E-mail: zhengjing2013@hnu.edu.cn (J.Z.)
*E-mail: Yangrh@pku.edu.cn (R.Y.).

Author Contributions

$^{\perp}$Z.Z. and C.L. contributed equally to this work.

Notes

The authors declare no competing financial interest.

DOI: 10.1021/acsami.5b00368
ACS Appl. Mater. Interfaces 2015, 7, 6211−6219

■ ACKNOWLEDGMENTS

We are grateful for financial support through the National Natural Science Foundation of China (21405038, 21135001, and 21305036), the Foundation for Innovative Research Groups of NSFC (21221003), the "973" National Key Basic Research Program (2011CB91100-0), and the Fundamental Research Funds for the Central Universities.

■ REFERENCES

(1) Peer, D.; Karp, J. M.; Hong, S.; Farokhzad, O. C.; Margalit, R.; Langer, R. Nanocarriers as an Emerging Platform for Cancer Therapy. *Nat. Nanotechnol.* **2007**, *2*, 751−760.

(2) Davis, M. E.; Chen, Z.; Shin, D. M. Nanoparticle Therapeutics: an Emerging Treatment Modality for Cancer. *Nat. Rev. Drug Discovery* **2008**, *7*, 771−782.

(3) Kamaly, N.; Xiao, Z.; Valencia, P. M.; Radovic-Moreno, A. F.; Farokhzad, O. C. Targeted Polymeric Therapeutic Nanoparticles: Design, Development and Clinical Translation. *Chem. Soc. Rev.* **2012**, *41*, 2971−3010.

(4) Kim, J.; Park, S.; Lee, J. E.; Jin, S. M.; Lee, J. H.; Lee, I. S.; Yang, I.; Kim, J. S.; Kim, S. K.; Cho, M. H. Designed Fabrication of Multifunctional Magnetic Gold Nanoshells and Their Application to Magnetic Resonance Imaging and Photothermal Therapy. *Angew. Chem., Int. Ed.* **2006**, *45*, 7754−7758.

(5) Xu, C.; Xie, J.; Ho, D.; Wang, C.; Kohler, N.; Walsh, E. G.; Morgan, J. R.; Chin, Y. E.; Sun, S. Au-Fe_3O_4 Dumbbell Nanoparticles as Dual-functional Probes. *Angew. Chem., Int. Ed.* **2008**, *47*, 173−176.

(6) Liong, M.; Lu, J.; Kovochich, M.; Xia, T.; Ruehm, S. G.; Nel, A. E.; Tamanoi, F.; Zink, J. I. Multifunctional Inorganic Nanoparticles for Imaging, Targeting, and Drug Delivery. *ACS Nano* **2008**, *2*, 889−896.

(7) Park, J. H.; von Maltzahn, G.; Zhang, L. L.; Schwartz, M. P.; Ruoslahti, E.; Bhatia, S. N.; Sailor, M. J. Magnetic Iron Oxide Nanoworms for Tumor Targeting and Imaging. *Adv. Mater.* **2008**, *20*, 1630−1635.

(8) Lee, J. H.; Huh, Y. M.; Jun, Y.; Seo, J.; Jang, J.; Song, H. T.; Kim, S.; Cho, E. J.; Yoon, H. G.; Suh, J. S. Artificially Engineered Magnetic Nanoparticles for Ultra-Sensitive Molecular Imaging. *Nat. Med.* **2007**, *13*, 95−99.

(9) Michalet, X.; Pinaud, F. F.; Bentolila, L. A.; Tsay, J. M.; Doose, S.; Li, J. J.; Sundaresan, G.; Wu, A. M.; Gambhir, S. S.; Weiss, S. Quantum Dots for Live Cells, in Vivo Imaging, and Diagnostics. *Science* **2005**, *307*, 538−544.

(10) Lai, C. Y.; Trewyn, B. G.; Jeftinija, D. M.; Jeftinija, K.; Xu, S.; Jeftinija, S.; Lin, V. S. Y. A Mesoporous Silica Nanosphere-Based Carrier System with Chemically Removable CdS Nanoparticle Caps for Stimuli-Responsive Controlled Release of Neurotransmitters and Drug Molecules. *J. Am. Chem. Soc.* **2003**, *125*, 4451−4459.

(11) Aznar, E.; Marcos, M. D.; Martinez-Manez, R.; Sancenon, F.; Soto, J.; Amoros, P.; Guillem, C. pH- and Photo-Switched Release of Guest Molecules from Mesoporous Silica Supports. *J. Am. Chem. Soc.* **2009**, *131*, 6833−6843.

(12) Liu, R.; Zhang, Y.; Feng, P. Y. Multiresponsive Supramolecular Nanogated Ensembles. *J. Am. Chem. Soc.* **2009**, *131*, 15128−15129.

(13) Ashley, C. E.; Carnes, E. C.; Phillips, G. K.; Padilla, D.; Durfee, P. N.; Brown, P. A.; Hanna, T. N.; Liu, J. W.; Phillips, B.; Carter, M. B. The Targeted Delivery of Multicomponent Cargos to Cancer Cells by Nanoporous Particle-Supported Lipid Bilayers. *Nat. Mater.* **2011**, *10*, 389−397.

(14) Slowing, I. I.; Trewyn, B. G.; Giri, S.; Lin, V. S. Y. Mesoporous Silica Nanoparticles for Drug Delivery and Biosensing Applications. *Adv. Funct. Mater.* **2007**, *17*, 1225−1236.

(15) Trewyn, B. G.; Slowing, I. I.; Giri, S.; Chen, H. T.; Lin, V. S. Y. Synthesis and Functionalization of a Mesoporous silica Nanoparticle Based on the Sol-Gel Process and Applications in Controlled Release. *Acc. Chem. Res.* **2007**, *40*, 846−853.

(16) Vivero-Escoto, J. L.; Slowing, I. I.; Trewyn, B. G.; Lin, V. S. Y. Mesoporous Silica Nanoparticles for Intracellular Controlled Drug Delivery. *Small* **2010**, *6*, 1952−1967.

(17) Tasciotti, E.; Liu, X. W.; Bhavane, R.; Plant, K.; Leonard, A. D.; Price, B. K.; Cheng, M. M. C.; Decuzzi, P.; Tour, J. M.; Robertson, F. Mesoporous Silicon Particles as a Multistage Delivery System for Imaging and Therapeutic Applications. *Nat. Nanotechnol.* **2008**, *3*, 151−157.

(18) Saha, S.; Leung, K. C. F.; Nguyen, T. D.; Stoddart, J. F.; Zink, J. I. Nanovalves. *Adv. Funct. Mater.* **2007**, *17*, 685−693.

(19) Slowing, I. I.; Vivero-Escoto, J. L.; Wu, C. W.; Lin, V. S. Y. Mesoporous Silica Nanoparticles as Controlled Release Drug Delivery and Gene Transfection Carriers. *Adv. Drug Delivery Rev.* **2008**, *60*, 1278−1288.

(20) Climent, E.; Marcos, M. D.; Martinez-Manez, R.; Sancenon, F.; Soto, J.; Rurack, K.; Amoros, P. The Determination of Methylmercury in Real Samples Using Organically Capped Mesoporous Inorganic Materials Capable of Signal Amplification. *Angew. Chem., Int. Ed.* **2009**, *48*, 8519−8522.

(21) Murphy, C. J.; Gole, A. M.; Stone, J. W.; Sisco, P. N.; Alkilany, A. M.; Goldsmith, E. C.; Baxter, S. C. Gold Nanoparticles in Biology: Beyond Toxicity to Cellular Imaging. *Acc. Chem. Res.* **2008**, *41*, 1721−1730.

(22) Zhao, W. A.; Karp, J. M. Tumour Targeting: Nanoantennas Heat Up. *Nat. Mater.* **2009**, *8*, 453−454.

(23) Chang, Y. T.; Liao, P. Y.; Sheu, H. S.; Tseng, Y. J.; Cheng, F. Y.; Yeh, C. S. Near-Infrared Light-Responsive Intracellular Drug and siRNA Release Using Au Nanoensembles with Oligonucleotide-Capped Silica Shell. *Adv. Mater.* **2012**, *24*, 3309−3314.

(24) Zhang, Z. J.; Wang, L. M.; Wang, J.; Jiang, X. M.; Li, X. H.; Hu, Z. J.; Ji, Y. H.; Wu, X. C.; Chen, C. Y. Mesoporous Silica Coated Gold Nanorods as a Light Mediated Multifunctional Theranostic Platform for Cancer Treatment. *Adv. Mater.* **2012**, *24*, 1418−1423.

(25) Li, N.; Yu, Z. Z.; Pan, W.; Han, Y. Y.; Zhang, T. T.; Tang, B. A Near-Infrared Light-Triggered Nanocarrier with Reversible DNA Valves for Intracellular Controlled Release. *Adv. Funct. Mater.* **2013**, *23*, 2255−2262.

(26) Yang, X. J.; Liu, X.; Liu, Z.; Pu, F.; Ren, J. S.; Qu, X. G. Near-Infrared Light-Triggered, Targeted Drug Delivery to Cancer Cells by Aptamer Gated Nanovehicles. *Adv. Mater.* **2012**, *24*, 2890−2895.

(27) Chen, C. E.; Zhou, L.; Geng, J.; Ren, J. S.; Qu, X. G. Photosensitizer-Incorporated Quadruplex DNA-Gated Nanovechicles for Light-triggered, Targeted Dual Drug Delivery to Cancer Cells. *Small* **2013**, *9*, 2793−2800.

(28) Zhang, P. H.; Cheng, F. F.; Zhou, R.; Cao, J. T.; Li, J. J.; Burda, C.; Min, Q. H.; Zhu, J. J. DNA-Hybrid-Gated Multifunctional Mesoporous Silica Nanocarriers for Dual-Targeted and MicroRNA-Responsive Controlled Drug Delivery. *Angew. Chem., Int. Ed.* **2014**, *53*, 2371−2375.

(29) Zhou, S. W.; Du, X. Z.; Cui, F. B.; Zhang, X. F. Multi-Responsive and Logic Controlled Release of DNA Gated Mesoporous Silica Vehicles Functionalized with Intercalators for Multiple Delivery. *Small* **2014**, *10*, 980−988.

(30) Hu, B.; Zhao, Y.; Zhu, H. Z.; Yu, S. H. Selective Chromogenic Detection of Thiol-Containing Biomolecules Using Carbonaceous Nanospheres Loaded with Silver Nanoparticles as Carrier. *ACS Nano* **2011**, *5*, 3166−3171.

(31) Yuan, X.; Tay, Y. Q.; Dou, X. Y.; Luo, Z. T.; Leong, D. T.; Xie, J. P. Glutathione-Protected Silver Nanoclusters as Cysteine-Selective Fluorometric and Colorimetric Probe. *Anal. Chem.* **2013**, *85*, 1913−1919.

(32) Ran, X.; Sun, H. J.; Pu, F.; Ren, J. S.; Qu, X. G. Ag Nanoparticle-Decorated Graphene Quantum Dots for Label-Free, Rapid and Sensitive Detection of Ag^+ and Biothiols. *Chem. Commun.* **2013**, *49*, 1079−1081.

(33) Verma, A.; Simard, J. M.; Worrall, J. W. E.; Rotello, V. M. Tunable Reactivation of Nanoparticle-Inhibited β-Galactosidase by Glutathione at Intracellular Concentrations. *J. Am. Chem. Soc.* **2004**, *126*, 13987−13991.

(34) Vosch, T.; Antoku, Y.; Hsiang, J. C.; Richards, C. I.; Gonzalez, J. I.; Dickson, R. M. Strongly Emissive Individual DNA-Encapsulated Ag

DOI: 10.1021/acsami.5b00368
ACS Appl. Mater. Interfaces 2015, 7, 6211−6219

Nanoclusters as Single-Molecule Fluorophores. *Proc. Natl. Acad. Sci. U.S.A.* **2007**, *104*, 12616−12621.
(35) de Souza, N. All that Glitters but Does not Blink. *Nat. Methods* **2007**, *4*, 540−540.
(36) Gorelikov, I.; Matsuura, N. Single Step Coating of Mesoporous Silica on Cetyltrimethyl Ammonium Bromide-Capped Nanoparticles. *Nano Lett.* **2008**, *8*, 369−373.
(37) Shen, S.; Tang, H. Y.; Zhang, X. T.; Ren, J. F.; Pang, Z. Q.; Wang, D. G.; Gao, H. L.; Qian, Y. Targeting Mesoporous Silica-Encapsulated Gold Nanorods for Chemo-Photothermal Therapy with Near-Infrared Radiation. *Biomaterials* **2013**, *34*, 3150−3158.
(38) Liu, R.; Zhang, Y.; Zhao, X.; Agarwal, A.; Mueller, L. J.; Feng, P. Y. pH-Responsive Nanogated Ensemble Based on Gold-Capped Mesoporous Silica Through an Acid-Labile Acetal Linker. *J. Am. Chem. Soc.* **2010**, *132*, 1500−1501.
(39) Deng, L.; Ouyang, X. Y.; Jin, J. Y.; Ma, C.; Jiang, Y.; Yang, R. H. Exploiting the Higher Specificity of Silver Amalgamation: Selective Detection of Mercy (II) by Forming Ag/Hg Amalgam. *Anal. Chem.* **2013**, *85*, 8594−8600.
(40) Ye, X. C.; Jin, L. H.; Caglayan, H.; Chen, J.; Xing, G. Z.; Zheng, C.; Doan-Nguyen, V.; Kang, Y. J.; Engheta, N.; Kagan, C. R. Improved Size-Tunable Synthesis of Monodisperse Gold Nanorods Through the Use of Aromatic Additives. *ACS Nano* **2012**, *6*, 2804−2817.
(41) Barth, B. M.; Altinoglu, I. E.; Shanmugavelandy, S. S.; Kaiser, J. M.; Keasey, N. R.; Adair, J. H. Targeted Indocyanine-Green-Loaded Calcium Phosphosilicate Nanoparticles for in Vivo Photodynamic Therapy of Leukemia. *ACS Nano* **2011**, *5*, 5325−5337.
(42) Xiao, Z.; Shangguan, D.; Cao, Z.; Fang, X.; Tan, W. Cell-Specific Internalization Study of an Aptamer from Whole Cell Selection. *Chem.—Eur. J.* **2008**, *14*, 1769−1775.
(43) Hong, R.; Han, G.; Fernandez, J. M.; Kim, B. J.; Forbes, N. S.; Rotello, V. M. Glutathione-Mediated Delivery and Release Using Monolayer Protected Nanoparticle Carriers. *J. Am. Chem. Soc.* **2006**, *128*, 1078−1079.
(44) Deng, R. R.; Xie, X. J.; Vendrell, M.; Chang, Y. T.; Liu, X. G. Intracellular Glutathione Detection Using MnO_2-Nanosheet-Modified Upconversion Nanoparticles. *J. Am. Chem. Soc.* **2011**, *133*, 20168−20171.

DOI: 10.1021/acsami.5b00368
ACS Appl. Mater. Interfaces 2015, 7, 6211−6219